CDDpress

www.nature.com/cdd

ARTICLE

Check for updates

Foxk1 promotes bone formation through inducing aerobic glycolysis

Chungeng Liu[1,2,3,5], Naibo Feng[1,2,3,5], Zhenmin Wang[2], Kangyan Zheng[2], Yongheng Xie[1,2], Hongyu Wang[1,2], Houqing Long[1,2,4]✉ and Songlin Peng[1,2,4]✉

Transcription factor Foxk1 can regulate cell proliferation, differentiation, metabolism, and promote skeletal muscle regeneration and cardiogenesis. However, the roles of Foxk1 in bone formation is unknown. Here, we found that Foxk1 expression decreased in the bone tissue of aged mice and osteoporosis patients. Knockdown of Foxk1 in primary murine calvarial osteoblasts suppressed osteoblast differentiation and proliferation. Conditional knockout of Foxk1 in preosteoblasts and mature osteoblasts in mice exhibited decreased bone mass and mechanical strength due to reduced bone formation. Mechanistically, we identified Foxk1 targeted the promoter region of many genes of glycolytic enzyme by CUT&Tag analysis. Lacking of Foxk1 in primary murine calvarial osteoblasts resulted in reducing aerobic glycolysis. Inhibition of glycolysis by 2DG hindered osteoblast differentiation and proliferation induced by Foxk1 overexpression. Finally, specific overexpression of Foxk1 in preosteoblasts, driven by a preosteoblast specific osterix promoter, increased bone mass and bone mechanical strength of aged mice, which could be suppressed by inhibiting glycolysis. In summary, these findings reveal that Foxk1 plays a vital role in the osteoblast metabolism regulation and bone formation stimulation, offering a promising approach for preventing age-related bone loss.

Cell Death & Differentiation; https://doi.org/10.1038/s41418-024-01371-w

INTRODUCTION

Osteoporosis is a prevalent disease characterized by loss of bone mass and degeneration of bone microarchitecture, leading to an increased risk of fractures and difficulties in fracture recovery [1, 2]. As an age-related degenerative disease, the incidence of osteoporosis is rising significantly with the global aging population, posing a substantial burden on public health [3]. Bone undergoes continuous dynamic remodeling, regulated by the number and activity of bone-forming osteoblasts and bone-resorbing osteoclasts. Osteoblasts, essential for the growth and maintenance of the skeleton, play a crucial role in bone formation. A major function of osteoblasts is to synthesize extracellular matrix and to support mineralization [4].

Osteoblast dysfunction caused by aging leads the imbalance of bone formation and bone resorbing, resulting in occurrence of osteoporosis [5, 6]. Antiresorptive drug, e.g. bisphosphonates, has been widely used and achieved satisfactory curative effect in reducing fracture rates, however it cannot be applied for a long term due to the risk of atypical femoral fractures [7]. And bisphosphonates are unable to improve age-related bone formation loss, which is harmful to bone quality. Parathyroid hormone (PTH) and Wnt signaling are classical accelerant of bone formation [8]. Although antibody treatment against sclerostin and intermittent low-dose PTH treatment to induce Wnt signaling has been used to enhance osteoblast activity, the cost and risk of side effects limit their widespread application [9, 10]. Consequently, there remains a clinical need for additional therapeutics that safely stimulates osteoblast number and function.

Forkhead box (FOX) proteins are a superfamily of evolutionarily conserved transcription factors that are characterized by their "Forkhead" or "winged-helix" DNA binding domain [11]. Fox family comprise of 19 subfamilies (Foxa to Foxs) based on sequence homology [12]. Fox members are widely expressed in various tissues and regulate multiple cellular functions, including cell proliferation, differentiation, metabolism, and carcinogenesis, playing an important role in many diseases [13–16]. Foxk1 is one of the two members, Foxk1 and Foxk2, of the Foxk family [17]. Previous studies showed that Foxk1 play a vital role in myogenic stem cell differentiation and proliferation, and is essential for muscle regeneration [18, 19]. Foxk1 promotes cardiogenesis by regulating embryonic stem cell differentiation [20]. Furthermore, Foxk1 involves in cancer initiation, proliferation, invasion and metastasis [11]. Nevertheless, the role for Foxk1 in osteoblast function and bone formation is unknown and warrants further investigation.

Here, we identify Foxk1 as a critical manipulator of osteoblast metabolism regulation and bone formation. We found that conditional knockout of Foxk1 in preosteoblasts or mature

[1]Division of Spine, Department of Orthopedic Surgery, Shenzhen People's Hospital (The Second Clinical Medical College, Jinan University; The First Affiliated Hospital, Southern University of Science and Technology), Shenzhen 518020 Guangdong, China. [2]Shenzhen Key Laboratory of Musculoskeletal Tissue Reconstruction and Function Restoration, Shenzhen, China. [3]The First Affiliated Hospital, Jinan University, Guangzhou 510630, China. [4]Shenzhen Clinical Research Centre for Geriatrics, Shenzhen People's Hospital, Shenzhen, China. [5]These authors contributed equally: Chungeng Liu, Naibo Feng. ✉email: houqinglong@163.com; pengsonglin@mail.sustech.edu.cn

Received: 24 April 2024 Revised: 9 August 2024 Accepted: 27 August 2024
Published online: 05 September 2024

osteoblasts in mice impaired bone formation and overexpression of Foxk1 in preosteoblasts increased bone mass and mechanical strength of aged mice by promoting bone formation. We also demonstrated that Foxk1 triggers osteoblast differentiation and proliferation, and bone formation through the induction of aerobic glycolysis in osteoblasts. Collectively, our data highlight the previously unknown role for Foxk1 in osteoblast function and bone formation, and provide a potential target for preventing age-related bone loss.

RESULTS

Foxk1 involved in age-related osteoporosis and osteogenesis

To investigate whether Foxk1 is a functional molecule in osteoporosis, we examined its expression patterns in bone tissues of 3 month (3 m)- and 12 month (12 m)-old mice. Analysis of distal femur metaphysis by microCT revealed that reduced bone mass in 12m-old mice (Supplementary Fig. S1A). The bone volume (BV), bone volume/tissue volume ratio (BV/TV) and trabecular number (Tb.N) were significantly reduced in 12m-old mice compared to 3m-old (Supplementary Fig. S1B–D, $n = 4$ per group), while the trabecular separation (Tb.Sp) increased (Supplementary Fig. S1E, $n = 4$ per group). The expression of Foxk1 was decreased in 12m-old mice (Fig. 1A ($n = 3$ per group) and 1B), with the reduced osteogenic markers expression, Runx2 and Osterix (Fig. 1B). Immunofluorescence (IF) staining images showed a remarkable reduction of Osterix and Foxk1 positive cell (Supplementary Fig. S1F). We next collected the bone tissue samples from individuals diagnosed with osteoporosis and from control subjects to investigate the expression of Foxk1. The results demonstrated that Foxk1 was also remarkably decreased in samples with osteoporosis (Fig. 1C ($n = 6$ per group) and 1D). To further examine the dynamic expression of Foxk1 during osteogenesis in vitro, primary murine calvarial osteoblasts were isolated and induced osteoblast differentiation. We found that the expression of osteogenic markers, Runx2, Osterix and alkaline phosphatase (Alp) increased during osteoblast differentiation (Supplementary Fig. S1G). The gradually enhanced Alp staining further confirmed osteoblast differentiation (Supplementary Fig. S1H). qPCR and Western blot revealed that Foxk1 expression significantly increased on the third day (day 3) of osteoblast differentiation and remained at a high level on day 7 (Fig. 1E ($n = 3$ per group) and Supplementary Fig. S1I). The above results suggested that Foxk1 is associated with osteoporosis and osteogenesis.

Foxk1 positively regulates osteoblast differentiation and proliferation

To determine the intrinsic role of Foxk1 in osteoblasts, we examined the differentiation and proliferation of primary murine calvarial osteoblasts knocked down of Foxk1 or not by siRNA. The introduction of siFoxk1 resulted in a reduction of Foxk1 mRNA expression (Fig. 1F, $n = 3$ per group), which is consistent with the protein reduction (Fig. 1K). Knockdown of Foxk1 decreased the osteogenic marker genes expression, including Runx2, Osterix, Alp, and osteocalcin (Ocn) (Fig. 1G–J, $n = 3$ per group). These findings were further confirmed by introducing siFoxk1 into primary murine calvarial osteoblast cultures, which decreased RUNX2 and OSTERIX protein levels (Fig. 1K). Furthermore, cells treated with siFoxk1 displayed significant inhibition of ALP and Alizarin Red S (ARS) staining (Fig. 1L, M). Then, we investigated the proliferation of osteoblasts by examining Edu incorporation and IF staining of cell cycle marker Ki67, and found that knockdown of Foxk1 displayed a significant reduction in Edu incorporation and the percentage of Ki67 positive cells in primary murine calvarial osteoblast (Fig. 1N, O, $n = 3$ per group). These results indicated that Foxk1 is required for osteoblast differentiation and proliferation.

Deletion of Foxk1 in Preosteoblasts leads to low bone mass and strength

To understand the role of Foxk1 in osteogenesis in vivo, the *Osx-cre* transgenic mice were mated with *Foxk1*$^{fl/fl}$ mice to deplete Foxk1 from committed osteoblast progenitors (Supplementary Fig. S2A). IF staining images showed that the osterix positive cells significantly decreased in *Osx-cre;Foxk1*$^{fl/fl}$ mice, with the reduction of Foxk1 (Supplementary Fig. S2B), which coincide with knockdown of Foxk1 inhibiting osteoblast proliferation. Immunohistochemical (IHC) staining further confirmed the successful deletion of Foxk1 (Supplementary Fig. S2C). Male and female *Osx-cre;Foxk1*$^{fl/fl}$ mice at 4 weeks of age were smaller and lighter than their *Osx-cre* littermates (Supplementary Fig. S2D, E, G and H, $n = 8$ per group). Analysis of femur metaphysis with microCT showed that Foxk1 deletion impaired the bone mass (Fig. 2A, B) and decreased the BV, BV/TV, and Tb.N compared to control mice (Fig. 2C (*Osx-cre* mice: $n = 7$; *Osx-cre;Foxk1*$^{fl/fl}$ mice: $n = 8$) and 2D ($n = 8$ per group)). In addition, Foxk1 knockout also led to significant elevation of Tb.Sp (Fig. 2C, D). Next, the trabecular bone area and number, determined by H&E staining, were reduced in *Osx-cre;Foxk1*$^{fl/fl}$ mice compared to *Osx-cre* littermates (Supplementary Fig. S2J, L). Biomechanical testing showed that *Osx-cre;Foxk1*$^{fl/fl}$ mice exhibited an overall deterioration in biomechanical properties characterized by markedly reduced maximum force, maximum bending strength, and elastic modulus (Supplementary Fig. S2F, I, Fig. 2E, F, $n = 7$ per group).

Next, calcein double labeling was used to analyze the bone formation ability in *Osx-cre;Foxk1*$^{fl/fl}$ mice. The results shewed that bone formation activity was lower in the *Osx-cre;Foxk1*$^{fl/fl}$ mice than the *Osx-cre* mice, indicated as slower mineral apposition rate (MAR) and bone formation rate (BFR) (Fig. 2G, H, $n = 3$ per group). OCN IHC staining revealed shrunk number of osteoblasts on trabecular bone surface in *Osx-cre;Foxk1*$^{fl/fl}$ mice compared to *Osx-cre* mice (Fig. 2I, J, $n = 5$ per group), which is consistent with the reduced ossification and bone formation rate. Interestingly, Tartrate resistant acid phosphatase (TRAP) staining indicated that the osteoclast number showed no obvious differences between groups in male *Osx-cre;Foxk1*$^{fl/fl}$ mice, whereas, the osteoclast number significantly decreased in female (Supplementary Fig. S2N, O, $n = 5$ per group). ELISA showed that Foxk1 knockout did not affect the level of C-terminal telopeptides of type I collagen (CTX-1) in male mice, but it reduced its level in female mice (Supplementary Fig. S2K, M, $n = 6$ per group).

Loss of Foxk1 in osteoblasts causes reduced bone mass and strength

To explore how Foxk1 functioned in mature osteoblasts in vivo, we deleted Foxk1 in mature osteoblasts using *Ocn-Cre* (Supplementary Fig. S3A). The results demonstrated that deletion of Foxk1 resulted in Ocn positive cells significantly decreased with the reduction of Foxk1 (Supplementary Fig. S3B), suggesting that Foxk1 regulates the proliferation of mature osteoblasts. IHC staining of Foxk1 further confirmed the successful deletion (Supplementary Fig. S3C). Knockout of Foxk1 did not affect the body size (data not shown) and body weight in both male and female mice at 4 weeks of age (Supplementary Fig. S3D ($n = 7$ per group) and Supplementary Fig. S3G ($n = 8$ per group)). Analysis of femur metaphysis with microCT demonstrated that the bone mass (Fig. 3A, B) and the BV, BV/TV, and Tb.N showed a significant reduction in *Ocn-Cre;Foxk1*$^{fl/fl}$ mice compared to *Ocn-Cre* mice, while the Tb.Sp was elevated (Fig. 3C ($n = 7$ per group) and 3D ($n = 8$ per group)). And we found that the trabecular bone area and number were reduced in *Osx-cre;Foxk1*$^{fl/fl}$ mice compared to *Osx-cre* littermates by H&E staining (Supplementary Fig. S3J, K). Biomechanical testing reveled that deletion of Foxk1 impaired the biomechanical properties of femur (Fig. 3E, F, Supplementary Fig. S3E, H, $n = 6$ per group). Dynamic histomorphometric analysis

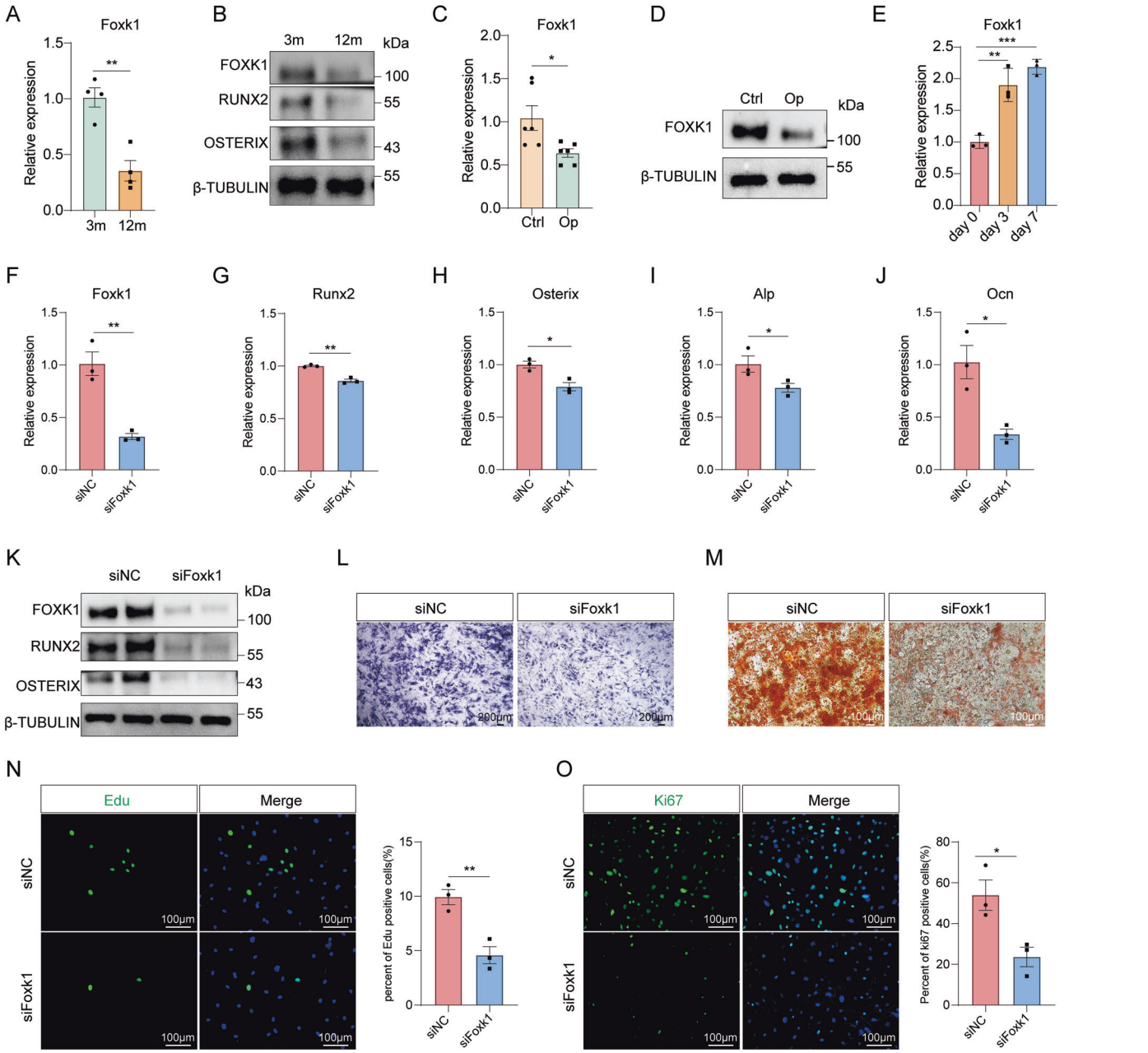

Fig. 1 Knockdown of Foxk1 inhibited osteoblast differentiation and proliferation. A qPCR analysis of mRNA levels of Foxk1 in femurs of 3 months (3 m) and 12m-old mice ($n = 3$ per group). **B** Western blot analysis of FOXK1, RUNX2 and OSTERIX protein from 3 m and 12m-old mice femur. **C** qPCR analysis of mRNA levels of Foxk1 in bone tissues of osteoporosis patients and controls ($n = 6$ per group). **D** Western blot analysis and quantification of FOXK1 from bone tissues of osteoporosis patients and controls. **E** qPCR analysis of mRNA levels of Foxk1 in primary murine calvarial osteoblasts at day 0, day 3 and day 7 during osteoblast differentiation ($n = 3$ per group). **F–J** qPCR was used to quantify Foxk1, Runx2, Osterix, Alp and Ocn mRNA levels after 7 days of siRNA transfection in primary murine calvarial osteoblasts ($n = 3$ per group). **K** Western blot analysis of FOXK1, RUNX2 and OSTERIX protein levels in primary murine calvarial osteoblasts after transfection with siNC or siFoxk1 for 7 days. **L** Representative images of ALP staining of primary murine calvarial osteoblasts after transfection with siRNA for 7 days. **M** Representative images of ARS staining of primary murine calvarial osteoblasts after transfection with siRNA for 14 days. **N** Representative images and quantification of Edu incorporation in primary murine calvarial osteoblasts after transfection with siRNA for 3 days ($n = 3$ per group). **O** Representative images and quantification of Ki67 IF staining in primary murine calvarial osteoblasts after transfection with siRNA for 3 days ($n = 3$ per group). *$p < 0.05$, **$p < 0.01$, ***$p < 0.001$.

of calcein double labeling revealed that bone formation activity remarkably decreased in the *Ocn-cre;Foxk1*$^{fl/fl}$ mice than the *Ocn-cre* mice, manifested as slower MAR and BFR (Fig. 3G, H, $n = 3$ per group). In addition, the osteopenic manifestations of the *Ocn-cre;Foxk1*$^{fl/fl}$ mice was further confirmed by the decrease in osteoblast numbers (Fig. 3I, J, $n = 5$ per group). The osteoclast number and bone resorption showed no obvious differences between groups in male mice (Supplementary Fig. S3L ($n = 5$ per group) and Supplementary Fig. S3F ($n = 6$ per group)), however these showed a reduction in female *Ocn-cre;Foxk1*$^{fl/fl}$ mice (Supplementary Fig. S3M ($n = 5$ per group) and Supplementary Fig. S3I ($n = 6$ per group)).

Taken together, these findings demonstrated that osteoblastic Foxk1 positively regulates the function of osteoblasts and bone

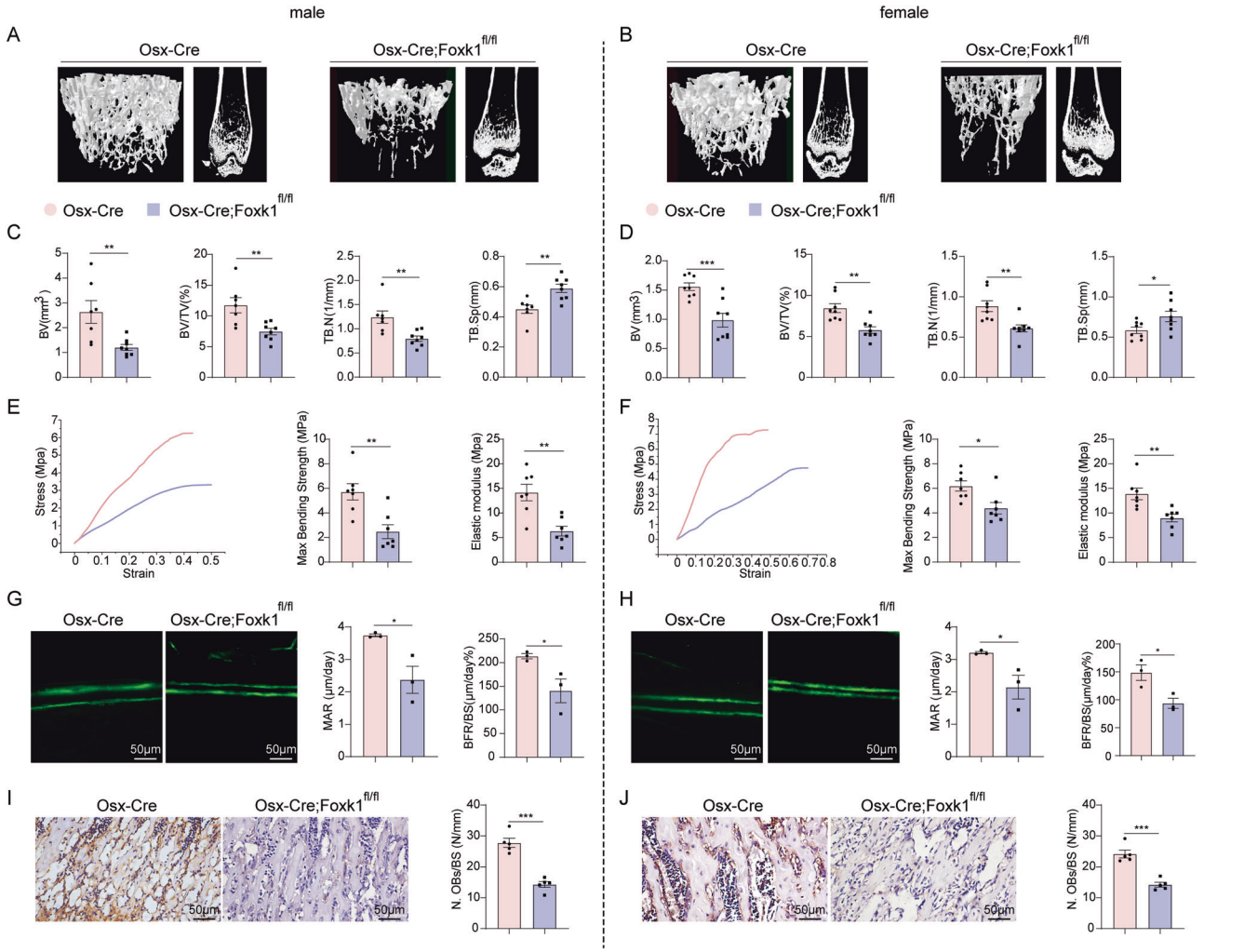

Fig. 2 Loss of Foxk1 in preosteoblasts leads to low bone mass and strength. Representative images of microCT analysis of male (**A**) and female (**B**) *Osx-cre;Foxk1*$^{fl/fl}$ mice and corresponding controls including two-dimensional construction of distal femur and three-dimensional reconstruction of trabecular bone of distal femur at 4 weeks old. Quantification of microCT analyses of the femur distal end from male (**C**) and female (**D**) *Osx-cre;Foxk1*$^{fl/fl}$ mice and corresponding controls at 4 weeks old (male: $n = 7$ for *Osx-cre* mice and $n = 8$ for *Osx-cre;Foxk1*$^{fl/fl}$ mice; female: $n = 8$ per group). Biomechanical properties analysis of the left femur from male (**E**) and female (**F**) *Osx-cre;Foxk1*$^{fl/fl}$ mice and corresponding controls at 4 weeks old ($n = 7$ per group). Dynamic osteogenic index of trabecular bone, including MAR and BFR, from the femoral metaphysis in male (**G**) and female (**H**) *Osx-cre;Foxk1*$^{fl/fl}$ mice and corresponding controls at 4 weeks old ($n = 3$ per group). Representative images and quantification of OCN IHC staining in male (**I**) and female (**J**) *Osx-cre;Foxk1*$^{fl/fl}$ mice and corresponding controls at 4 weeks old ($n = 5$ per group). *$p < 0.05$, **$p < 0.01$.

formation, and controls ossification and proliferation both in preosteoblasts and mature osteoblasts in vivo.

Foxk1 is involved in regulating aerobic glycolysis in osteoblasts

Next, we performed the Cleavage Under Targets and Tagmentation (CUT&Tag) assay of primary murine calvarial osteoblasts to assess the DNA-binding profiles of transcription factor Foxk1. Global mapping analysis showed that Foxk1 peaks were mainly observed at or near transcription start site (TSS) (Supplementary Fig. S4A). We identified 5961 genomic Foxk1 binding sites, of which 73.11% were localized on the promoter regions (Supplementary Fig. S4B). Kyoto encyclopedia of genes and genomes (KEGG) analysis of Foxk1 binding genes showed that significant enrichment in glycolysis/glycogenesis signaling pathways (Fig. 4A). Specifically, the promoter region of several rate-limiting enzyme genes of glycolysis, including hexokinase-2 (Hk2), phosphofructokinase muscle isoform (Pfkl, Pfkp, and Pfkfb3), pyruvate kinase (Pkm), and enolase 1 (Eno1), were enrichment (Fig. 4B). Notably, Foxk1 could bind to the promoter region of pyruvate dehydrogenase kinases 1 (Pdk1) (Fig. 4B), which can phosphorylate regulatory subunit E1α of the pyruvate dehydrogenase complex (PDC) to inhibit its enzymatic activity. The link between Foxk1 and these enzyme genes was confirmed by qPCR after chromatin immunoprecipitation (ChIP) (Supplementary Fig. S4C, $n = 3$ per group). Foxk1 knockdown decreased the expression of Hk2, Pfkl, Pfkp, Pfkfb3, Eno1, Pkm, and Pdk1 in primary murine calvarial osteoblasts (Supplementary Fig. S4D, $n = 3$ per group). *Osx-cre;Foxk1*$^{fl/fl}$ mice showed a significant reduction of these glycolytic gene expression in femur (Supplementary Fig. S4E, $n = 5$ per group).

Positive regulation of glycolytic genes by Foxk1 led us to investigate the role of Foxk1 in glycolysis process. Knockdown of Foxk1 in primary murine calvarial osteoblasts significantly decreased glucose uptake (Fig. 4C, $n = 6$ per group). Seahorse glycolytic stress test demonstrated that Foxk1 knockdown caused a significant decrease of glycolysis, which was manifested by

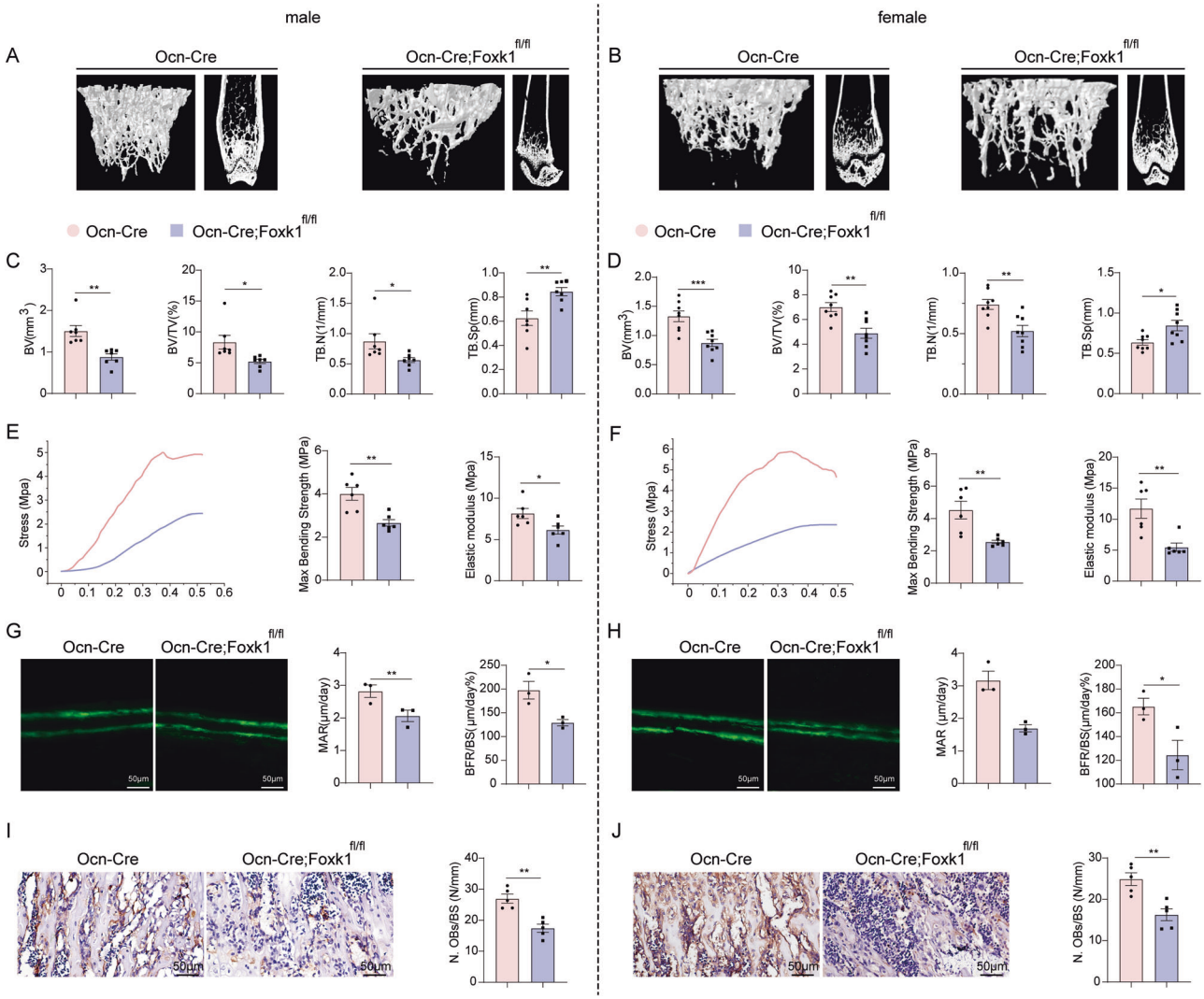

Fig. 3 Deletion of Foxk1 in mature osteoblasts results in low bone mass and strength. Representative images of microCT analysis of male (**A**) and female (**B**) *Ocn-cre;Foxk1*$^{fl/fl}$ mice and corresponding controls including two-dimensional construction of distal femur and three-dimensional reconstruction of trabecular bone of distal femur at 4 weeks old. Quantification of microCT analyses of the femur distal end from male (**C**) and female (**D**) *Ocn-cre;Foxk1*$^{fl/fl}$ mice and corresponding controls at 4 weeks old (male: $n = 7$ per group; female: $n = 8$ per group). Biomechanical properties analysis of the left femur from male (**E**) and female (**F**) *Ocn-cre;Foxk1*$^{fl/fl}$ mice and corresponding controls at 4 weeks old ($n = 6$ per group). Dynamic osteogenic index of trabecular bone, including MAR and BFR, from the femoral metaphysis in male (**G**) and female (**H**) *Ocn-cre;Foxk1*$^{fl/fl}$ mice and corresponding controls at 4 weeks old ($n = 3$ per group). Representative images and quantification of OCN IHC staining in male (**I**) and female (**J**) *Ocn-cre;Foxk1*$^{fl/fl}$ mice and corresponding controls at 4 weeks old ($n = 5$ per group). $^{*}p < 0.05$, $^{**}p < 0.01$.

extracellular acidification rate (ECAR) (Fig. 4D–F, $n = 6$ per group). Cells knocked down for Foxk1 showed a reduction in lactate concentration in culture medium, consistent with ECAR (Fig. 4G, $n = 4$ per group). And Foxk1 knockdown showed no obvious impact of mitochondrial respiration, examined by seahorse mitochondrial stress test (Supplementary Fig. S4F–H, $n = 6$ per group). Next, we performed metabonomic analysis in primary murine calvarial osteoblasts with Foxk1 knockdown, to detect intermediate metabolites of glycolysis pathways. Strikingly, our data confirm an inhibition of glycolysis caused by the suppression of Foxk1, with glucose 6-phosphate (G6-P), fructose 6-phosphate (F6-P), Fructose 1,6-bisphosphate (F1,6-P), 3-phosphoglyceric acid (3-PG), pyruvate and lactate remarkably decreased (Fig. 4H–M, $n = 6$ per group). Therefore, we found that Foxk1 controls the glycolytic pathway through multiple dimensions in osteoblasts (Fig. 4N). Thus, Foxk1 could positively regulate glycolysis in osteoblasts, even in oxygen rich conditions, called aerobic glycolysis.

Foxk1 regulates the osteoblast differentiation and proliferation by inducing glycolysis

Our next objective was to assess the role of glycolysis in osteoblast function. The results showed that glucose uptake, ECAR and lactate release significantly increased during osteoblast differentiation, indicating elevation of glycolysis (Supplementary Figs. S5A, S5E ($n = 3$ per group), Supplementary Fig. S5B–D ($n = 6$ per group)). Inhibition of glycolysis by 2-deoxy-Dglucose (2DG) suppressed the expression of osteogenic marker genes in osteoblasts (Supplementary Fig. S5G–J ($n = 3$ per group), Supplementary Fig. S5K). Interestingly, Foxk1 expression was elevated after glycolysis inhibiting (Supplementary Fig. S5F ($n = 3$ per group) and Supplementary Fig. S5K), which may be a negative feedback regulation. ALP and ARS staining were markedly reduced in cells treated with 2DG (Supplementary Fig. S5L). Edu incorporation and IF staining of Ki67 demonstrated that suppression of glycolysis significantly decreased the proliferation of osteoblasts (Supplementary Fig. S6A, B, $n = 3$ per group).

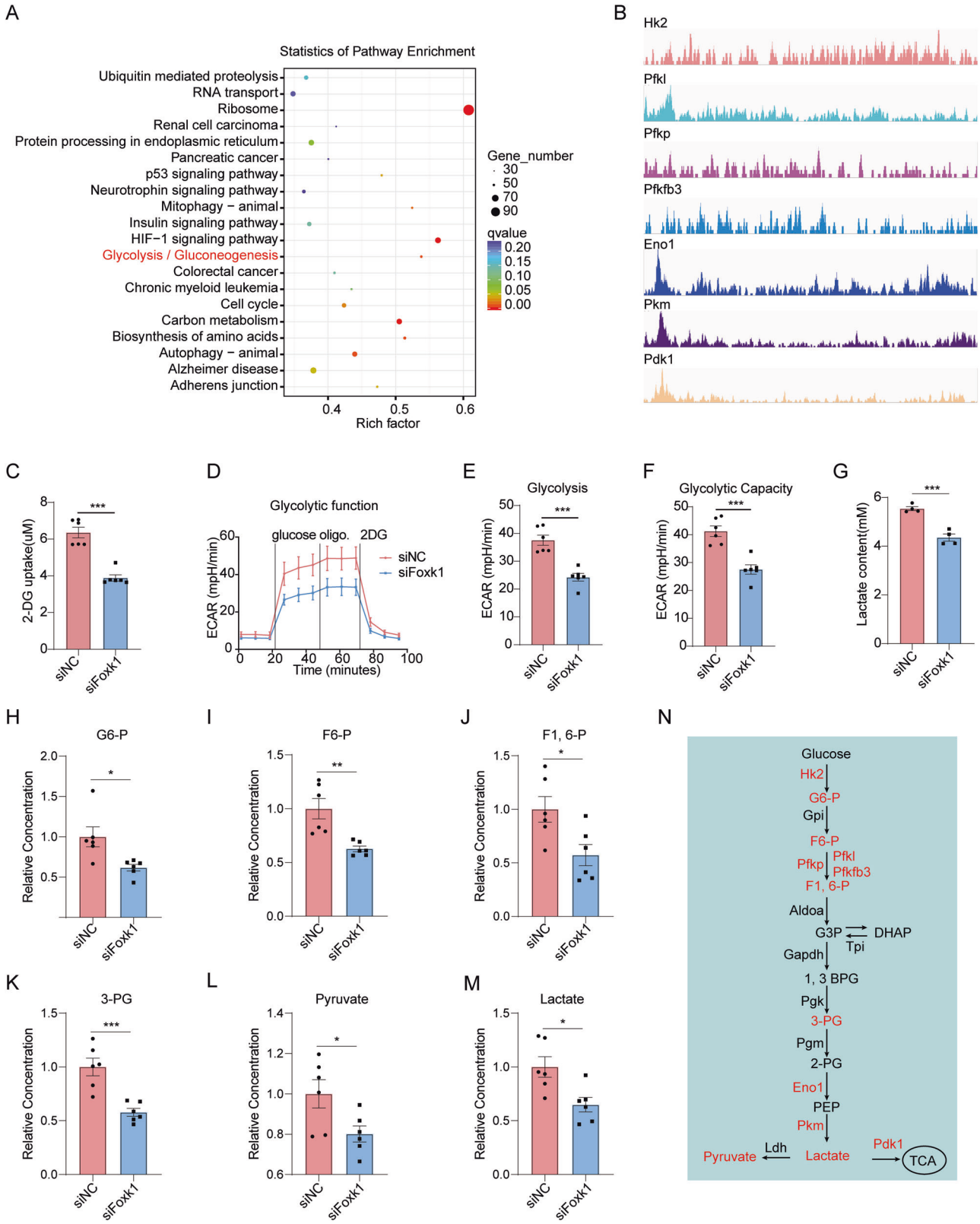

Subsequently, we examined whether Foxk1 regulates osteoblast function by enhancing glycolysis. We found that 2DG blocked the promoting effect of Foxk1 on osteoblast glycolysis (Fig. 5A–C ($n = 5$ per group) and Fig. 5D ($n = 6$ per group)). Inhibiting glycolysis weakened the enhanced osteogenic marker genes by overexpression of Foxk1 (Fig. 5E–H ($n = 3$ per group), Supplementary Fig. S6D). Reduction of ALP and ARS staining confirmed that the positive effect of Foxk1 on osteogenic differentiation was prevented by glycolysis inhibition (Fig. 5I, J). Edu incorporation and IF staining of Ki67 showed that Foxk1 could

Fig. 4 Foxk1 plays a critical role in regulating aerobic glycolysis of osteoblasts. A KEGG analysis of direct target genes from CUT&Tag-seq of Foxk1 overexpressing primary murine calvarial osteoblasts. **B** IGV visual analyzed the FOXK1 biding regions of its targeted genes. **C** Glucose uptake is determined in Foxk1 knockdown versus control primary murine calvarial osteoblasts ($n = 6$ per group). **D–F** The extracellular acidification rate (ECAR) in primary murine calvarial osteoblasts was measured using Seahorse XF assay, in response to Foxk1 knockdown. Glycolysis (**E**) and glycolytic capacity (**F**) were analyzed ($n = 6$ per group). **G** Lactate levels of medium cultured for Foxk1 knockdown and control primary murine calvarial osteoblasts was examined ($n = 4$ per group). **H–M** Metabonomic analysis glycolytic intermediate metabolites (G6-P, F6-P, F1,6-P, 3-PG, pyruvate and lactate) in primary murine calvarial osteoblasts with Foxk1 knockdown was performed ($n = 6$ per group). **N** Mapping of Foxk1-induced metabolic genes and metabolites within glycolytic pathways. The factors decreased in primary murine calvarial osteoblasts with Foxk1 knockdown are marked in red font. $^*p < 0.05$, $^{**}p < 0.01$, $^{***}p < 0.01$.

promote osteoblast proliferation, which was impeded by inhibition of glycolysis (Fig. 5K, L, Supplementary Fig. S6E, F, $n = 3$ per group). These results demonstrate that Foxk1 primarily enhances osteoblast differentiation and proliferation by promoting aerobic glycolysis.

Foxk1 increases the bone mass of aged mice through induction of glycolysis

To investigate the role of Foxk1 in age-related bone loss, we constructed an adeno-associated virus 9 (AAV9) that contained a preosteoblast-specific promoter (Osterix) to overexpress Foxk1 in preosteoblasts (AAV9-Osterix-Foxk1) (Supplementary Fig. S7A). We first aimed to examine the infection efficiency and function in vitro and incubated AAV9-Osterix-GFP (AAV9-GFP) and AAV9-Osterix-Foxk1 (AAV9-Foxk1) with primary murine calvarial osteoblasts and RAW cells. Transduced cells were evaluated for GFP expression by fluorescence microscopy and we found that AAV9-GFP transduced osteoblasts efficiently, but poorly in RAW cells (Supplementary Fig. S7B). The expression of Foxk1 showed a significant elevation in osteoblasts treated with AAV9-Foxk1, while represented a relatively unimpressive upregulation amplitude in RAW cells (Supplementary Fig. S7C ($n = 3$ per group) and Supplementary Fig. S7D). AAV9-Foxk1 infection increased the osteogenic marker gene expression, ALP staining and ARS staining, suggesting promotion of osteoblast differentiation (Supplementary Fig. S7E–H ($n = 3$ per group) and Supplementary Fig. S7I, J).

Next, to examine whether Foxk1 promotes bone formation through the upregulation of glycolysis in aged mice, 12m-old male mice were simultaneously injected with AAV9-Foxk1 and 2DG (12m-Foxk1-2DG) via tail vein (Fig. 6A). Whole body and individual organ imaging showed that the expression of GFP was highest in the hindlimbs, modest in liver and not detected in heart, spleen, lung, and kidney (Fig. 6B). Expression of GFP in the femur and liver was further confirmed by IF staining (Supplementary Fig. S8A). Notably, IF staining revealed that GFP colocalized with Osterix in femur (Fig. 6C), indicating that AAV9 could efficiently infect preosteoblasts. IHC staining showed that the expression of Foxk1 decreased in 12m-old mice femur compared to 3m-old mice, but treatment of AAV9-Foxk1 significantly increased Foxk1 expression and 2DG boosted this effect (Fig. 6D). qPCR confirmed the alteration of Foxk1 expression in the femur (Fig. 6E, $n = 3$ per group). And we found that the expression of Foxk1 increased in liver (Supplementary Fig. S8B, $n = 3$ per group), which corresponds with GFP expression (Fig. 6B and Supplementary Fig. S8A). No significant changes in histological features of heart, liver, spleen, lung, and kidney were observed in different groups (Supplementary Fig. S8C).

The MicroCT analysis demonstrated that glycolysis inhibition blocked the promoting effect of Foxk1 on bone mass (Fig. 6F), the BV, BV/TV, and Tb.N, and suppression effect on Tb.Sp (Fig. 6G–J, $n = 6$ per group). H&E staining revealed that the trabecular bone area and number were increased in AAV9-Foxk1 treated 12m-old mice (the group of 12m-Foxk1-PBS), which was prevented by 2DG administering (the group of 12m-Foxk1-2DG) (Supplementary Fig. S9A). Biomechanical testing reveled that glycolysis inhibiting suppressed the elevation of the femur biomechanical properties in AAV9-Foxk1 treated 12m-old mice (Fig. 6K, L, $n = 6$ per group). Foxk1 overexpression improved the MAR and BFR in 12m-old mice, which could be attenuated by glycolysis inhibition (Fig. 6M–O, $n = 3$ per group). AAV9-Foxk1 treated mice displayed an increased number of osteoblasts, while administration of 2DG impeded this effect (Supplementary Fig. S9B, C, $n = 5$ per group). These data indicated that the promoting effect of Foxk1 on bone formation was counteracted by inhibition of glycolysis in aged mice. TRAP staining (Supplementary Fig. S9D, E, $n = 5$ per group) and Elisa of CTX-1 (Supplementary Fig. S9F, $n = 5$ per group) showed that the number of osteoclast and bone resorption presented no significant alteration in AAV9-GFP, AAV9-Foxk1 and 2DG treated groups. These findings collectively indicate that the protection effect of Foxk1 on age-related bone loss was mediated by enhancement of aerobic glycolysis.

DISCUSSION

Development of more efficient and safer regulatory targets that stimulate osteoblast number and differentiation to enhance bone formation is extraordinary important in improving treatment of osteoporosis. In the current study, we discovered that Foxk1 promote osteoblast differentiation and proliferation, and bone formation by enhancing aerobic glycolysis. Preosteoblast and mature osteoblast-specific knockout of Foxk1 deceased the bone mass and mechanical strength by weakening bone formation. Forcing the expression of Foxk1 in preosteoblasts improve the bone mass and mechanical strength in aged mice, which could be attenuated by glycolysis inhibitor 2DG. Consequently, our findings suggest that targeting Foxk1 could serve as a strategy for preventing age-related bone loss.

The transcription factors Foxk1 ubiquitously expressed in various tissues and organs and they play vital roles in cell function, including cell proliferation, cell differentiation and cell metabolism [11]. Foxk1 can regulate skeletal muscle by mediating myogenic stem cell proliferation and differentiation [18, 19, 21] and promote cardiogenesis by regulating Wnt signaling [20]. Recently, a report showed that Foxk1 regulate adipogenic differentiation of bone marrow stromal cells [22]. In addition, Foxk1 have been shown to have important roles in tumorigenesis [11]. Here we found that Foxk1 expression decreased in bone tissues of aged mice and osteoporosis patients, while gradually increased during osteoblast differentiation. These findings prompted us to investigate the role of Foxk1 in osteoblast function and bone formation. We knocked down Foxk1 in primary murine calvarial osteoblasts and found that Foxk1 has a positive role in regulating osteoblast differentiation and proliferation. Then, to conditionally knockout Foxk1 from preosteoblasts at the initial stage of differentiation and from mature osteoblast at late stage of differentiation, two lines of transgenic mice were generated by using different temporal markers of osteoblast, Osterix and Ocn [23]. We found that deletion of Foxk1 in both initial and late stage decreased bone mass and mechanical strength through suppressing bone formation, which indicates that Foxk1 is necessary for maintaining osteoblast differentiation in vivo at the whole period. To our knowledge, this is the first

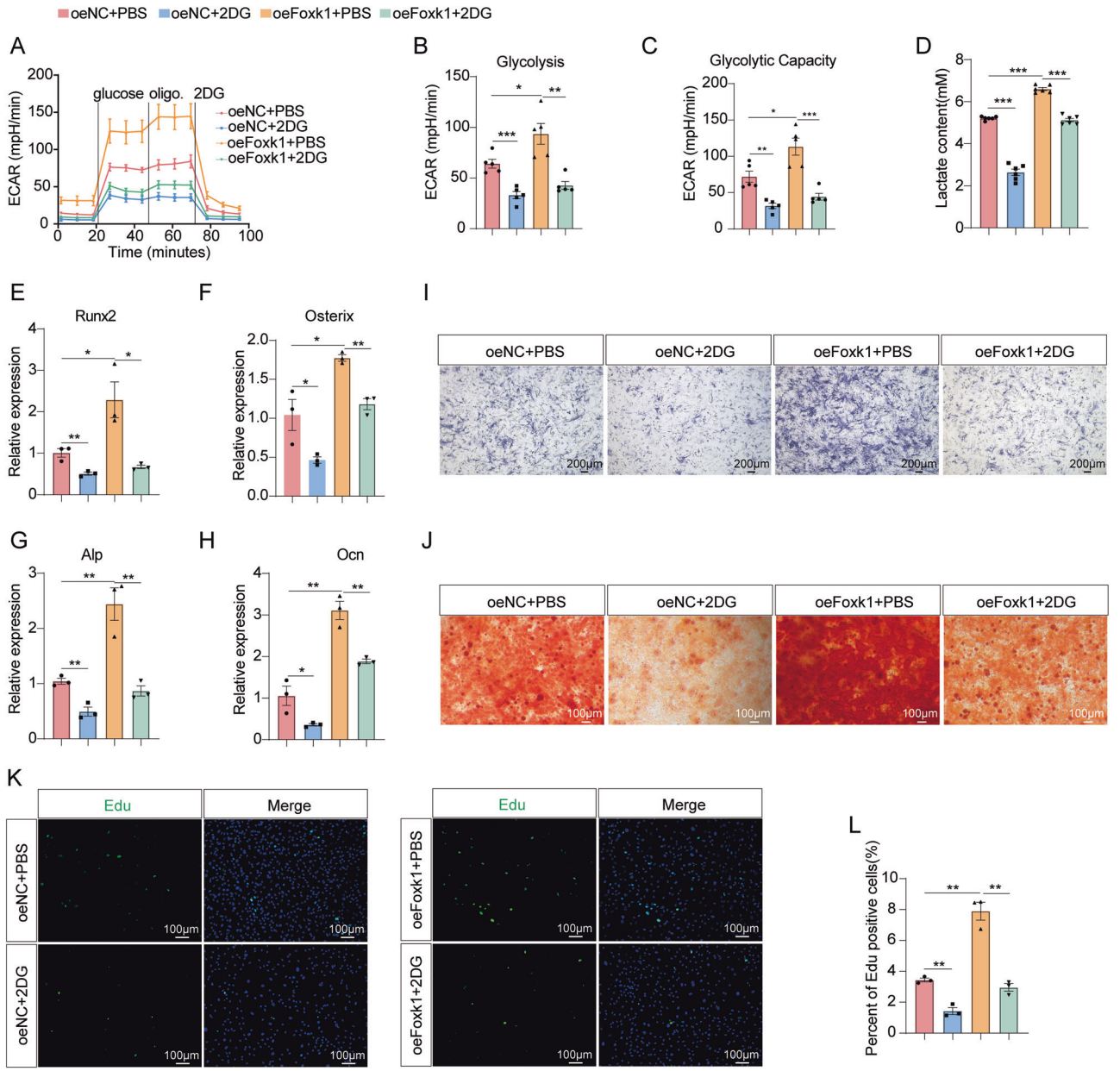

Fig. 5 Foxk1 regulation of osteoblast differentiation and proliferation relies on glycolysis. A–C The extracellular acidification rate (ECAR) in control (oeNC) and Foxk1 overexpressed (oeFoxk1) primary murine calvarial osteoblasts treated with PBS or 2DG was measured using Seahorse XF assay. Glycolysis (**B**) and glycolytic capacity (**C**) were analyzed ($n = 5$ per group). **D** Lactate levels of medium cultured for Foxk1 overexpressed primary murine calvarial osteoblasts and control treated with PBS or 2DG was examined ($n = 6$ per group). **E–H** mRNA levels of Runx2, Osterix, Alp, and Ocn in control and Foxk1 overexpressed primary murine calvarial osteoblasts treated with PBS or 2DG were quantified by qPCR ($n = 3$ per group). Representative images of ALP (**I**) and ARS (**J**) staining of control and Foxk1 overexpressed primary murine calvarial osteoblasts treated with PBS or 2DG. **K, L** Representative images and quantification of Edu incorporation in control and Foxk1 overexpressed primary murine calvarial osteoblasts treated with PBS or 2DG ($n = 3$ per group). *p < 0.05, **p < 0.01, ***p < 0.01.

report describing the roles of Foxk1 in osteoblast function and bone formation.

Foxk1 can promote aerobic glycolysis by targeting many glycolytic enzymes and inhibiting further oxidation of pyruvate in the mitochondria by increasing the activity of Pdk1 and Pdk4 in 3T3L1 adipocytes and L6 myoblasts [24]. Moreover, Foxk1 regulates multiple genes associated with glycolysis and downstream anabolic pathways and contribute to mTORC1-regulated metabolic reprogramming in mouse embryonic fibroblasts [25]. We discovered that FOXK1 protein could bind to promoter regions of several glycolytic enzyme genes in primary murine calvarial osteoblasts by using CUT&Tag, which is consistent with previous report [24, 25]. And we found that Foxk1 could regulate these glycolytic enzyme genes in vitro and in vivo. Furthermore, we found that Foxk1 could positively regulate aerobic glycolysis and knockdown of Foxk1 decreased glycolytic intermediates by applying metabonomic analysis. However, our data demonstrated that Foxk1 had no significant effect on mitochondrial oxidative metabolism.

Aerobic glycolysis produces 80% of the energy in mature osteoblasts and is a prominent feature of osteoblast differentiation [6, 26]. Stabilization of Hif1α drive bone formation by upregulation of glycolytic metabolism [27]. As classical accelerant of bone formation, PTH and Wnt signaling can promote osteoblast

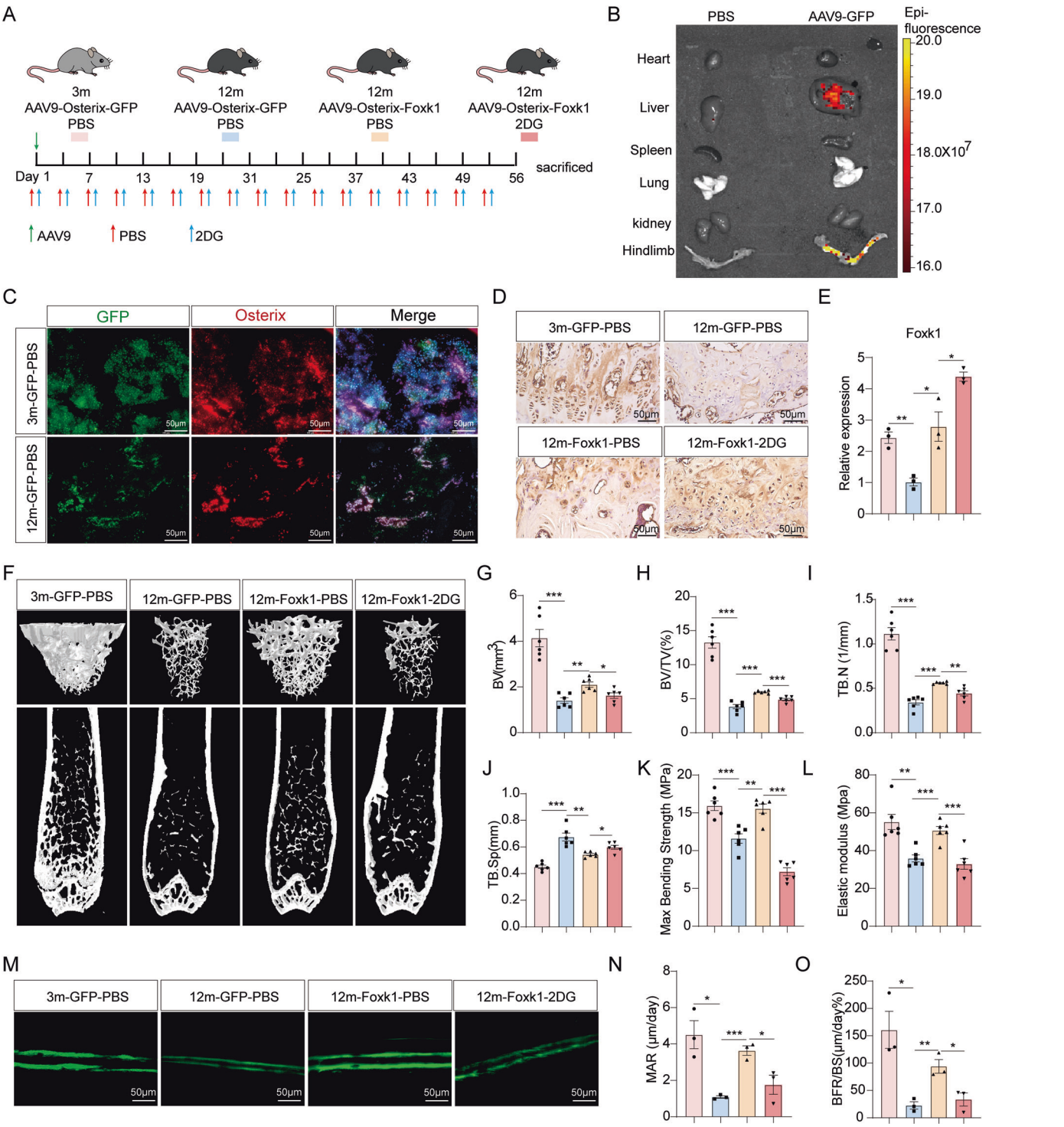

Fig. 6 Foxk1 increases the bone mass of aged mice through the induction of glycolysis. A Experimental design of the 12m-old mice treated with AAV9-Foxk1 and 2DG via tail vein injection. Femurs from different groups were collected for further analysis after 56 days of AAV9 treatment. **B** The IVIS-100 optical imaging system was used to monitor GFP expression in individual tissues. y-axis, radiant efficiency (p/s/cm^2/sr/μW/cm^2). **C** Representative IF staining images of GFP and Osterix in femur of 3 m and 12m-old mice treated with AAV9-GFP. **D** Representative images of FOXK1 IHC staining of the femurs from treated 3 m and 12m-old mice. **E** mRNA levels of Foxk1 in femurs from treated 3 m and 12m-old mice was quantified by qPCR ($n = 3$ per group). **F** Representative MicroCT images of two-dimensional image construction of distal femur and three-dimensional image reconstruction of trabecular bone of distal femur from treated 3 m and 12m-old mice. **G**–**J** Quantification of microCT analyses of the femur distal end from treated 3 m and 12m-old mice ($n = 6$ per group). **K**, **L** Biomechanical properties analysis of the left femur from treated 3 m and 12m-old mice ($n = 6$ per group). **M**–**O** Dynamic osteogenic index of trabecular bone, including MAR (**N**) and BFR (**O**), from the femoral metaphysis in treated 3 m and 12 m mice ($n = 3$ per group). *$p < 0.05$, **$p < 0.01$, ***$p < 0.01$.

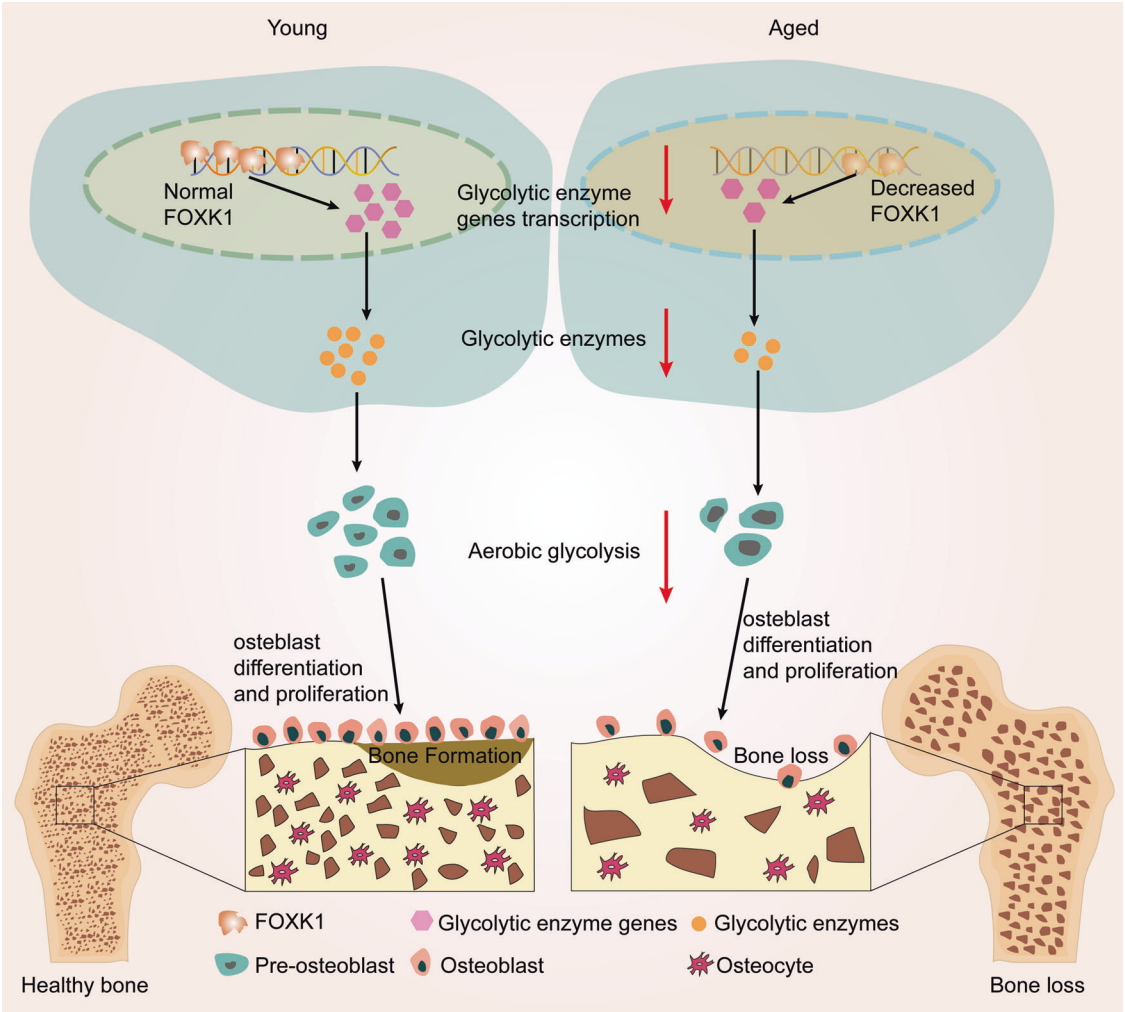

Fig. 7 A model of Foxk1 in osteogenesis and age-related bone loss. Foxk1 promotes transcription of several glycolytic genes and improve the level of glycolysis in osteoblasts, which induces osteoblast differentiation and proliferation and bone formation. In aged mice, the expression of Foxk1 is decreased in osteoblasts, resulting in suppression of glycolysis. Limited glycolysis weakens osteoblast differentiation and proliferation, which causes age-related bone loss.

differentiation and bone formation through aerobic glycolysis [6, 28–30]. Extracellular vesicles derived from skeletal muscle can promote osteogenesis by inducing aerobic glycolysis [31]. Our data further confirmed that aerobic glycolysis elevated with osteoblast differentiation. We found that inhibition of glycolysis blocked the osteogenesis mediated by the overexpression of Foxk1 in vitro, even if inhibiting glycolysis further increases the expression of Foxk1. The increase in Foxk1 expression caused by inhibition of glycolysis may be a negative feedback regulation, which has also been reported in previous studies [32–34]. Of course, the specific mechanism needs further experimental exploration. And we discovered that glycolysis is essential for Foxk1 triggering bone formation in vivo. Besides, we observed that glycolysis is necessary for inducing osteoblast proliferation by Foxk1. In fact, proliferative cells, like cancer cells, also rely on glycolysis to produce energy, a phenomenon termed “the Warburg effect” [35]. Providing more metabolic intermediates for synthesis of extracellular matrix or cellular components may be the reason of osteoblast prefer aerobic glycolysis when undergo differentiation and proliferation [6, 35]. Of course, more research is needed to explore this hypothesis.

In relevant preclinical and clinical studies, the AAV vector has a long-term record of safety and efficacy, because of their lack of pathogenicity [36]. AAV9 has been confirmed to have superior bone targeting properties, but AAV9 can target a wide range of tissues withal [37]. To solve this side-effect of AAV9, we engineered AAV9 vector genome using preosteoblast-specific promoter (Osterix) to transduce exclusively osteoblast lineage cells. We demonstrated that our engineered AAV9 vector possessed satisfactory osteoblast specificity in vitro and in vivo. We found that overexpression of Foxk1 in preosteoblasts by using AAV9 vector modified by promoter Osterix improved bone mass and mechanical strength through enhancing bone formation. And inhibition glycolysis could hinder Foxk1 promoted bone formation in aged mice, which further indicated that glycolysis plays a critical role in Foxk1 regulated osteogenesis. Thus, our findings demonstrated that Foxk1 can serve as a target for preventing age-related bone loss and provided an ideal gene therapy vectors for bone disease.

In conclusion, our study identified Foxk1 as a novel regulator of osteoblast metabolism and bone formation (Fig. 7). Conditional knockout of Foxk1 in osteoblast reduced bone formation in mice. Foxk1 enhanced osteoblast differentiation and proliferation by inducing glycolysis. Overexpression of Foxk1 in preosteoblasts improved bone mass and mechanical strength in aged mice through enhancing glycolysis. We provide a novel insight in the regulatory mechanism of bone formation and target of preventing age-related bone loss.

MATERIALS AND METHODS

Experimental animals

All animal experimentation conducted in this investigation received approval from the Animal Ethics Review Committee of Shenzhen People's Hospital, and all procedural interventions strictly adhered to its stipulated guidelines. The sample size of animal was minimized according to the animal care guidelines. The investigators responsible for histological analyses were blinded to group information. Mice were randomly assigned to the experimental groups.

Mice

WT C57BL/6J mice were obtained from SPF(BEIJING) BIOTECHNOLOGY CO., LTD. (Beijing, China). *Foxk1*$^{fl/+}$ mice were obtained from Professor Yu Nie of Fuwai Hospital, Chinese Academy of Medical Sciences. *Osterix-Cre* mice were purchased from BIOCYTOGEN (Shanghai, China). *Ocn-Cre* mice purchased from Cyagen Biosciences (Suzhou, China). To generate *Osx-cre;Foxk1*$^{fl/fl}$ and *Ocn-cre;Foxk1*$^{fl/fl}$ conditional knockout mice, *Osterix-Cre* and *Ocn-Cre* mice were crossed for over three generations with *Foxk1*$^{fl/+}$ mice. Tail genomic DNA is applied to identify the genotypes by PCR amplification. Genotype identification primers of the Foxk1 knockout allele and Cre transgene mice are listed in Supplementary Table S1. Specific pathogen free facilities were used to propagate and raise all mice.

MicroCT

Mouse right femurs were fixed in 4% paraformaldehyde and scanned with a MicroCT system (SkyScan 1276, Bruker, Belgium) at 80 kVp, 100 μA, exposure time 926 ms, and 20 μm pixels. NRecon software was used to construct a two-dimensional image of the distal femur and a three-dimensional image of the trabecular bone of the distal femur. The cylindrical area at the distal end of the growth plate is used to define the volume of interest (VOI) of the femur. The bone volume/tissue volume ratio (BV/TV), bone volume (BV), trabecular number (Tb.N) and trabecular separation (Tb.Sp) were analyzed.

ELISA

Blood collected from mice was centrifuged at 2000 × *g* for 30 min to harvest the plasma. The concentration of C-terminal telopeptides of type I collagen (CTX-1) (Jianglai Biology, JL20123, Shanghai, China) in the plasma was analyzed according to the manufacturer's instructions.

Bone biomechanical properties

Three-point bending mechanical strength devices (AG-IS, Shimadzu, Japan) were used to test the biomechanical properties as previous described [38]. Briefly, the left femur was obtained from mice and cleaned of adherent tissue. A three-point bending test was conducted at the mid-shaft of the femur wrapped in saline-soaked gauze. The femur was placed at two points 6 mm apart, and the test specimen was moved down at a speed of 1 mm/min. The biomechanical data were produced and analyzed to determine the max force, max bending strength, and elastic modulus.

Bone histomorphometry

In order to analyze dynamic behavior, mice were double labeled with calcein (20 mg/kg; Sigma-Aldrich, C0875, Missouri, USA) through intraperitoneal injection at 9 days and 3 days before sacrifice. The right femurs were dehydrated with 20% sucrose solution and performed frozen sectioning at a thickness of 10 μm to obtain frontal sections of the trabecular bone using a Leica SM2500E microtome (Leica Microsystems, Wetzlar Germany). Obtain fluorescence images using an inverted fluorescence microscope (Leica image analysis system, Q500MC). Then the dynamic bone formation parameters, including mineral apposition rate (MAR) and bone formation rate (BFR), were analyzed by ImageJ software (NIH, USA).

Immunohistochemical analyses

4% paraformaldehyde was used to fix the femur for 48 h, followed by 10% EDTA to decalcify it. Decalcified bones are dehydrated and then embedded in paraffin. A paraffin microtome (Leica, Wetzlar, Germany) is used to cut bone specimens into 5-μm-thick sections. The decalcified bone specimens were applied to perform H&E staining, IHC staining, IF staining and Trap staining.

IHC staining and IF staining were performed according to the protocol. After dewaxing, the slides were incubated overnight at 4 °C with the primary antibody. After incubating the secondary antibody at room temperature for one hour, take photos for testing. IHC staining for OCN was used to assess the number of OCN positive osteoblasts as previous described [39]. The numbers of osteoblasts on cancellous bone surface in the entire region of interest were counted and the data were then normalized to the number of osteoblasts per millimeter of trabecular bone surface perimeter (N mm^{-1}). Trap staining was used to assess the number of osteoclasts as previous described [39]. IHC and Trap staining images were obtained by light microscopy (TS2-S-SM; Nikon, Tokyo, Japan). IF staining images were obtained by an inverted fluorescence microscope (Leica image analysis system, Q500MC). FOXK1 (ab18196, 1:500) and GFP (ab290, 1:200) primary antibody were purchased from abcam (Cambridge, England). OCN (sc-390877, 1:200) and OSTERIX (sc-393325, 1:200) primary antibody were purchased from santa cruz biotechnology (California, USA). Anti-rabbit (A-11008, 1:400; A-11012, 1:400) and anti-mouse (A-11005, 1:400; A-11001, 1:400) secondary antibody were purchased from Invitrogen (California, USA). TRAP staining kit (387A) was purchased from Sigma Aldrich (Missouri, USA).

AAV9 construction and injection in mice

Adeno-associated virus-9 (AAV9) was used as a vector to overexpressed Foxk1 in mice. AAV9 vector was modified by preosteoblast specific promoter osterix to target exclusively osteoblast lineage cells, which was designed and synthetized by WZ Biosciences Inc. (Shangdong, China). 4×10^{11} GC AAV9 was diluted with PBS to 100 μl and injected into each mouse through the tail vein. Tail vein injection of 100 μl PBS as control group to perform Whole body and individual organ imaging of GFP expression and obtain tissues 2 weeks after injection. To investigate the role of glycolysis in Foxk1 mediated bone formation, 2DG (200 μl, 0.5 mg/g, Sigma-Aldrich, D8375) or PBS (200 μl) was injected every three days via intraperitoneal until the mice are euthanized at 8 weeks after virus injection according previous report [31].

Human samples

The bone samples of 12 man subjected to spinal fusion surgery in Shenzhen People's Hospital were employed in this research. The inclusion criteria are based on bone density manifested by T-score. Osteoporosis group ($n = 6$) consisted of individuals with low bone mineral density (T score ≤ -2.5 SD), while control group ($n = 6$) consisted of individuals with normal bone mineral density (T score ≥ -1.0 SD) [40]. Individuals with other bone diseases, including rheumatoid arthritis and osteoarthritis, were excluded from the research. The research ethics committee of Shenzhen People's Hospital approved this study. Each participant has signed an informed consent form.

Cell culture and osteoblast differentiation

Mouse calvaria of 1 to 3-day-old pups was applied to isolate Primary calvarial osteoblasts. Briefly, the collected calvarias were cut into pieces and incubated with 2.5% tryptase (Gibco, 25200072, New York, USA) at 37°C with gentle shaking for 10 min. Supernatant was discarded and type I collagenase (Biyotime, ST2294-100mg, Shanghai, China) was added to cover the calvaria at 37°C with gentle shaking for 30 min. Supernatant was discarded again and type I collagenase was added to cover the calvaria at 37°C with gentle shaking for 60 min. Then supernatant was collected and centrifuged 300 g for 5 minutes at room temperature. The precipitated cells were resuspended in α-MEM (Gibco, 12571063) with 10% fetal bovine serum (Gibco, 10099141 C) and incubated under 5% CO2 at 37°C overnight. The next day, replace the culture medium with a new one to remove non adherent cells.

For all experiments, the primary calvarial osteoblasts were incubated with osteogenic induction medium, as previous described [26], containing 10 mM b-glycerol phosphate (Sigma-Aldrich, G9422) and 50 ug/ml ascorbic acid (Sigma-Aldrich, A4544) and replace the culture medium every other day.

siRNA transfection and virus infection

The small interfering RNAs against Foxk1 (Table S4) and control siRNAs were designed and synthesized by Hanbio Co. Ltd (Shanghai, China). siRNAs were transfected into the primary calvarial osteoblasts after reaching ~80-90% confluency using Lipofectamine 2000 (Invitrogen, 11668027, California, USA) in accordance with the manufacturer's instructions.

The adenovirus of overexpression of Foxk1 and control adenovirus in cells were designed and synthesized by WZ Biosciences Inc. Adenovirus were added to the primary calvarial osteoblasts after reaching ~80-90% confluency with 2DG (2 mM) or PBS.

western blotting

To isolate protein, cells were scraped, or bones were pulverized in RIPA lysis buffer (Biyotime, P0013B) containing protease inhibitors (Biyotime, P1005). Protein concentration was measured using the BCA method and 10 μg of the protein was run on 12-14% SDS-PAGE gels (Yeasen Biotechnology, 36249ES10, Shanghai, China) and transferred to PVDF membranes (Millipore, IPVH00005, Massachusetts, USA). Then the PVDF membranes were blocked with TBST containing 5% dried skimmed milk and incubated with anti-FOXK1 (ab18196, 1:1000), anti-RUNX2 (1:500, Proteintech, 20700-1-AP, Wuhan, China), anti-OSTERIX (sc-393325, 1:500), anti-ALP (1:500, Proteintech, 60294-1-Ig) and anti-β-Tubulin (1:1000, Proteintech, 10094-1-AP) at 4°C overnight. Incubate the membranes containing the primary antibody with the HRP anti-rabbit secondary antibody (Proteintech, RGAR001, 1:5000) or HRP anti-mouse secondary antibody (Proteintech, RGAM001, 1:5000 for WB) at room temperature for 1 hour. Finally, the membranes were visualized using SuperSignal™ West Pico PLUS Chemiluminescent Substrate Reagent (Thermo Fisher Scientific, 34580 Massachusetts, USA).

qPCR

The RNeasy kit (Qiagen, 74104, Hilden, Germany) was used to extract Total RNA from cells, while TRIzol reagent (Invitrogen, 15596018CN) was applied in tissues, according to the manufacturers' instructions. RNA concentrations were determined using a Nano-Drop ND-2000 spectrophotometer (Thermo Fisher Scientific). Total 1000 ng RNA was performed Reverse transcription using the Prime Script™ Reverse Transcript Master Mix (TaKaRa Bio, RR037A, Otsu, Japan). qPCR was performed on a StepOnePlus Real-Time PCR system (Applied Biosystems, Waltham, USA). The relative mRNA concentrations were calculated by the $2^{-\Delta\Delta Ct}$ method and normalized to that of β-actin. The primers used for qPCR are listed in Table S2.

ALP and Alizarin red staining

ALP and Alizarin red staining was performed to examine the osteogenic ability of primary calvarial osteoblasts. Briefly, treated primary calvarial osteoblasts were induced osteogenic differentiation for 7days to perform ALP staining and for 14days to perform Alizarin red staining. Cells were washed twice at the corresponding time point and fix them with 4% paraformaldehyde for 10 min. Then ALP staining solution (Beyotime, P0321S) or Alizarin red S staining solution (Beyotime, C0140-100ml,) at pH 8.3 was used to stain the cells for 30 min. After washing twice, the cells were photographed by light microscopy (TS2-S-SM, Nikon, Japan).

Glucose uptake assays and lactate measurements

Glucose uptake of primary calvarial osteoblasts was detected by a Glucose uptake kit (abcam, ab136955) according to the instructions. Briefly, primary calvarial osteoblasts were seeded to 96-well plates and starved for 4 hours with α-MEM without FBS. Then, Cells were incubated with 10 mM 2DG for 20 min. Cells were Lysed after wash twice and interacted with reaction mix. Measure output at OD 412 nm on a microplate reader (TECAN, Spark 10 M, Switzerland). Uptake of glucose was normalized to the cell numbers.

Lactic Acid assay kit (Nanjing Jiancheng Bioengineering Institute, A019-1-1, Nanjing, China) was used to measure lactate levels in culture medium.

Measurement of extracellular acidification rate and oxygen consumption rate

The Extracellular Acidification Rate (ECAR) and Oxygen Consumption Rate (OCR) were measured by XF24 Extracellular Flux Analyzer (Seahorse Bioscience, Maine, USA) as previously described [41]. Briefly, a poly-L-lysine-coated XF24 V7 microplate (Seahorse Bioscience) was seeded with 70000 primary calvarial osteoblasts. Next, primary calvarial osteoblasts were treated with siNC, siFoxk1, or adenovirus for Foxk1 overexpression as described in the results. On the day of measurement, osteoblasts were washed twice with XF medium and incubated for 1 hour in a CO_2 free incubator at 37°C before loading. Glucose (25 mM), oligomycin (1 μM), FCCP (2 μM), antimycin A (0.5 μM), rotenone (0.5 μM), 2-deoxy-glucose (50 mM) and BSA:palmitate (200 μM) were used to measure ECAR (mpH/min) and OCR (pmol/min). Data were normalized to the cell numbers.

Metabolomics analysis

Primary calvarial osteoblasts were plated on 10 cm cell culture dish and knocked down Foxk1 using siRNA. Cells were harvested to detect energy metabolism related metabolites using Acquity-I Xevo TQ-S LCMs (Waters, Massachusetts, USA). Use MassLynx software (v4.1, Waters) to process the raw data files generated by UPLC-MS/MS, and perform peak search, integration, calibration, and quantification for each metabolite.

Cell proliferation detection

Primary calvarial osteoblasts were seeded in 24 well plate size cell crawling plate. Next, primary calvarial osteoblasts were treated with siNC, siFoxk1, or adenovirus for Foxk1 overexpression as described in the results. Then cells were collected to perform Edu incorporation (Yeasen Biotechnology, 40275ES60, Shanghai, China) according to the instructions or IF staining of Ki67 (abcam, ab16667) to evaluate osteoblast proliferation. Obtain fluorescence images using an inverted fluorescence microscope (Leica image analysis system, Q500MC).

CUT&Tag

Primary calvarial osteoblasts were seeded in 12 well plate and over-expressed Foxk1 using adenovirus. Cells were collected to perform CUT&Tag using a Hyperactive Universal CUT&Tag Assay Kit for Illumina (Vazyme Biotechnolegy, TD903-01, Nanjing, China) after 72 hours treatment according to the manufacturer's protocol. Briefly, Cells were collected and resuspended with 100 μl wash buffer. Cell suspension incubated with activated ConA Beads for 10 min at room temperature. The supernatant was discarded after instantaneous centrifugation and resuspended with 50 μl precooled antibody buffer containing 1 μg anti-FOXK1 antibody (abcam, ab18196). Cell suspension was placed at 4°C overnight. The supernatant was discarded and sediment incubated with 50 μl Dig-wash Buffer containing secondary antibody for 60 min at room temperature with rotation. The supernatant was discarded and sediment incubated with 100 μl Dig-300 Buffer containing 2 μl pA/G-Tnp for 60 min at room temperature. The supernatant was discarded and sediment incubated with 50 μl Dig-300 Buffer containing 10 μl 5×TTBL for 60 min at 37°C to make fragmentation of chromatin. Chromatin fragmentation incubated with 5 μl Proteinase K, 100 μl Buffer L/B and 20 μl DNA Extract Beads for 10 min at 55°C. The supernatant was discarded and beads were washed twice with Buffer WA and Buffer WB respectively. The supernatant was discarded and DNA eluted with 22 μl sterilized ultrapure water. Then, Libraries were amplified and sequenced on Illumina Novaseq platform at Novogene Science and Technology Co., Ltd (Beijing, China) and 150 bp paired-end reads were generated.

Data obtained from CUT&Tag of Foxk1 was analyzed as described previously with modifications [42]. To clean raw fastq reads, fastp (version 0.20.0) was used first. Clean reads obtained from CUT&Tag of Foxk1 were aligned to the reference genome using BWA (v0.7.12) mem. Further analysis only used unique mapped (MAPQ 13) and de-duplicated reads. MACS2 (version 2.1.0) was used for all peak calling. Peaks with q-value threshold of 0.05 was used for all data sets. Peak summit positions around transcription start sites can be used to predict protein-gene interaction sites. The nearest genes around the peak were retrieved and genomic region of the peak was annotated by ChIPseeker. KEGG pathways were statistically enriched for peak related genes using KOBAS software. IGV was used to perform visualization of peak distribution along genomic regions of interested genes.

ChIP assay

Primary calvarial osteoblasts were seeded in 15 cm cell culture dish and overexpressed Foxk1 using adenovirus. Cells were collected to perform ChIP using a SimpleChIP® Enzymatic Chromatin IP Kit (Cell Signaling Technology, 9003, Massachusetts, USA) after 72 hours treatment according to the manufacturer's protocol. In brief, 37% formaldehyde solution was used to crosslink protein and DNA of each sample. Cells were harvested and then added SDS lysis buffer with protease inhibitor cocktail. Chromatin was digested by enzyme and ultrasound. Chromatin fragments were incubated with 1 μg primary antibody of anti-FOXK1 (abcam, ab18196) or anti-IgG (Cell Signaling Technology, 9003) at 4°C overnight. DNA samples were precipitated with beads and quantified with specific primers (Table S3) via qPCR.

Statistical analysis

Prism 8 (GraphPad software) was used for statistical analysis, and data are presented as mean ± SEM. Statistical significance was determined by unpaired two-tailed Student's *t*-test for independent sample tests or one-way ANOVA followed by Tukey's multiple comparisons test for multiple comparisons. $P < 0.05$ was considered significant.

DATA AVAILABILITY

All data and material that support this study are available upon requests to the corresponding authors. The CUT&Tag data generated in this study have been deposited in the NCBI database under accession code PRJNA1093607.

REFERENCES

1. Eisman JA, Bogoch ER, Dell R, Harrington JT, McKinney RE, McLellan A, et al. Making the first fracture the last fracture: ASBMR task force report on secondary fracture prevention. J Bone Miner Res. 2012;27:2039–46.
2. Wang Y, Deng P, Liu Y, Wu Y, Chen Y, Guo Y, et al. Alpha-ketoglutarate ameliorates age-related osteoporosis via regulating histone methylations. Nat Commun. 2020;11:5596.
3. Rachner TD, Khosla S, Hofbauer LC. Osteoporosis: now and the future. Lancet. 2011;377:1276–87.
4. Esen E, Long F. Aerobic glycolysis in osteoblasts. Curr Osteoporos Rep. 2014;12:433–8.
5. Feng X, McDonald JM. Disorders of bone remodeling. Ann Rev Pathol. 2011;6:121–45.
6. Lee W-C, Guntur AR, Long F, Rosen CJ. Energy Metabolism of the Osteoblast: Implications for Osteoporosis. Endocr Rev. 2017;38:255–66.
7. Reid IR, Billington EO. Drug therapy for osteoporosis in older adults. Lancet. 2022;399:1080–92.
8. Russow G, Jahn D, Appelt J, Märdian S, Tsitsilonis S, Keller J. Anabolic Therapies in Osteoporosis and Bone Regeneration. Int J Mol Sci. 2018;20:83.
9. Neer RM, Arnaud CD, Zanchetta JR, Prince R, Gaich GA, Reginster JY, et al. Effect of parathyroid hormone (1-34) on fractures and bone mineral density in postmenopausal women with osteoporosis. N Engl J Med. 2001;344:1434–41.
10. Clarke BL. Anti-sclerostin antibodies: utility in treatment of osteoporosis. Maturitas. 2014;78:199–204.
11. Liu Y, Ding W, Ge H, Ponnusamy M, Wang Q, Hao X, et al. FOXK transcription factors: Regulation and critical role in cancer. Cancer Lett. 2019;458:1–12.
12. Lam EWF, Brosens JJ, Gomes AR, Koo C-Y. Forkhead box proteins: tuning forks for transcriptional harmony. Nat Rev Cancer. 2013;13:482–95.
13. Everson JL, Fink DM, Yoon JW, Leslie EJ, Kietzman HW, Ansen-Wilson LJ, et al. Sonic hedgehog regulation of Foxf2 promotes cranial neural crest mesenchyme proliferation and is disrupted in cleft lip morphogenesis. Development. 2017;144:2082–91.
14. van Gastel N, Stegen S, Eelen G, Schoors S, Carlier A, Daniëls VW, et al. Lipid availability determines fate of skeletal progenitor cells via SOX9. Nature. 2020;579:111–7.
15. Wilhelm K, Happel K, Eelen G, Schoors S, Oellerich MF, Lim R, et al. FOXO1 couples metabolic activity and growth state in the vascular endothelium. Nature. 2016;529:216–20.
16. Shan L, Zhou X, Liu X, Wang Y, Su D, Hou Y, et al. FOXK2 Elicits Massive Transcription Repression and Suppresses the Hypoxic Response and Breast Cancer Carcinogenesis. Cancer Cell. 2016;30:708–22.
17. Ji Z, Donaldson IJ, Liu J, Hayes A, Zeef LAH, Sharrocks AD. The forkhead transcription factor FOXK2 promotes AP-1-mediated transcriptional regulation. Mol Cell Biol. 2012;32:385–98.
18. Garry DJ, Meeson A, Elterman J, Zhao Y, Yang P, Bassel-Duby R, et al. Myogenic stem cell function is impaired in mice lacking the forkhead/winged helix protein MNF. Proc Natl Acad Sci USA 2000;97:5416–21.
19. Shi X, Wallis AM, Gerard RD, Voelker KA, Grange RW, DePinho RA, et al. Foxk1 promotes cell proliferation and represses myogenic differentiation by regulating Foxo4 and Mef2. J Cell Sci. 2012;125:5329–37.
20. Sierra-Pagan JE, Dsouza N, Das S, Larson TA, Sorensen JR, Ma X, et al. FOXK1 regulates Wnt signalling to promote cardiogenesis. Cardiovasc Res. 2023;119:1728–39.
21. Li C, Shen H, Liu M, Li S, Luo Y. Natural antisense RNA Foxk1-AS promotes myogenic differentiation by inhibiting Foxk1 activity. Cell Commun Signal. 2022;20:77.
22. Zhang S, You Y, Li Y, Yuan H, Zhou J, Tian L, et al. Foxk1 stimulates adipogenic differentiation via a peroxisome proliferator-activated receptor gamma 2-dependent mechanism. FASEB J. 2023;37:e23266.
23. Wei J, Shimazu J, Makinistoglu MP, Maurizi A, Kajimura D, Zong H, et al. Glucose Uptake and Runx2 Synergize to Orchestrate Osteoblast Differentiation and Bone Formation. Cell. 2015;161:1576–91.
24. Sukonina V, Ma H, Zhang W, Bartesaghi S, Subhash S, Heglind M, et al. FOXK1 and FOXK2 regulate aerobic glycolysis. Nature. 2019;566:279–83.
25. He L, Gomes AP, Wang X, Yoon SO, Lee G, Nagiec MJ, et al. mTORC1 Promotes Metabolic Reprogramming by the Suppression of GSK3-Dependent Foxk1 Phosphorylation. Mol Cell. 2018;70:949–60.e4.
26. Lee W-C, Ji X, Nissim I, Long F. Malic Enzyme Couples Mitochondria with Aerobic Glycolysis in Osteoblasts. Cell Rep. 2020;32:108108.
27. Regan JN, Lim J, Shi Y, Joeng KS, Arbeit JM, Shohet RV, et al. Up-regulation of glycolytic metabolism is required for HIF1α-driven bone formation. Proc Natl Acad Sci USA 2014;111:8673–8.
28. Esen E, Lee S-Y, Wice BM, Long F. PTH Promotes Bone Anabolism by Stimulating Aerobic Glycolysis via IGF Signaling. J Bone Miner Res. 2015;30:1959–68.
29. Esen E, Chen J, Karner CM, Okunade AL, Patterson BW, Long F. WNT-LRP5 signaling induces Warburg effect through mTORC2 activation during osteoblast differentiation. Cell Metab. 2013;17:745–55.
30. Karner CM, Long F. Wnt signaling and cellular metabolism in osteoblasts. Cell Mol Life Sci. 2017;74:1649–57.
31. Ma S, Xing X, Huang H, Gao X, Xu X, Yang J, et al. Skeletal muscle-derived extracellular vesicles transport glycolytic enzymes to mediate muscle-to-bone crosstalk. Cell Metab. 2023;35:2028–43.e7.
32. Hu Y, Tang J, Xu F, Chen J, Zeng Z, Han S, et al. A reciprocal feedback between N6-methyladenosine reader YTHDF3 and lncRNA DICER1-AS1 promotes glycolysis of pancreatic cancer through inhibiting maturation of miR-5586-5p. J Exp Clin Cancer Res. 2022;41:69.
33. Liu Y, He D, Xiao M, Zhu Y, Zhou J, Cao K. Long noncoding RNA LINC00518 induces radioresistance by regulating glycolysis through an miR-33a-3p/HIF-1α negative feedback loop in melanoma. Cell Death Dis. 2021;12:245.
34. Tangseefa P, Martin SK, Chin PY, Breen J, Mah CY, Baldock PA, et al. The mTORC1 complex in pre-osteoblasts regulates whole-body energy metabolism independently of osteocalcin. Bone Res. 2021;9:10.
35. Vander Heiden MG, Cantley LC, Thompson CB. Understanding the Warburg effect: the metabolic requirements of cell proliferation. Science. 2009;324:1029–33.
36. Basner-Tschakarjan E, Mingozzi F. Cell-Mediated Immunity to AAV Vectors, Evolving Concepts and Potential Solutions. Front Immunol. 2014;5:350.
37. Yang Y-S, Xie J, Wang D, Kim J-M, Tai PWL, Gravallese E, et al. Bone-targeting AAV-mediated silencing of Schnurri-3 prevents bone loss in osteoporosis. Nat Commun. 2019;10:2958.
38. Yang Y-Y, Zhou Y-M, Xu J-Z, Sun L-H, Tao B, Wang W-Q, et al. Lgr4 promotes aerobic glycolysis and differentiation in osteoblasts via the canonical Wnt/β-catenin pathway. J Bone Miner Res. 2021;36:1605–20.
39. Liu J-H, Chen C-Y, Liu Z-Z, Luo Z-W, Rao S-S, Jin L, et al. Extracellular Vesicles from Child Gut Microbiota Enter into Bone to Preserve Bone Mass and Strength. Adv Science. 2021;8:2004831.
40. Sun M, Hu L, Wang S, Huang T, Zhang M, Yang M, et al. Circulating MicroRNA-19b Identified From Osteoporotic Vertebral Compression Fracture Patients Increases Bone Formation. J Bone Miner Res. 2020;35:306–16.
41. Park S, Chang C-Y, Safi R, Liu X, Baldi R, Jasper JS, et al. ERRα-Regulated Lactate Metabolism Contributes to Resistance to Targeted Therapies in Breast Cancer. Cell Rep. 2016;15:323–35.
42. Kaya-Okur HS, Wu SJ, Codomo CA, Pledger ES, Bryson TD, Henikoff JG, et al. CUT&Tag for efficient epigenomic profiling of small samples and single cells. Nat Commun. 2019;10:1930.

ACKNOWLEDGEMENTS

We would like to thank Professor Yu Nie of Fuwai Hospital, Chinese Academy of Medical Sciences, for providing the *Foxk1*$^{fl/+}$ mice.

AUTHOR CONTRIBUTIONS

SP and HL designed and supervised the entire project. CL and NF wrote the draft of this manuscript. HL and SP were responsible for patient recruitment, surgical procedures, and sample collection. CL and NF performed most of the experiments. ZW, KZ, YX, and HW conducted partial experiments. CL and NF analyzed the data. All authors discussed the results and commented on the paper.

FUNDING

This work was supported by the National Natural Science Foundation of China (82272488, 82472413 and 82302031), the China Postdoctoral Science Foundation (2023M732376 and 2024M752135), the Shenzhen People's Hospital Clinician Scientist Training "Five Three" Plan Project (SYWGSJCYJ202302), the Guangdong Basic and Applied Basic Research Fund Shenzhen Joint Fund of China (2022A1515111197) and Natural Science Foundation of Guangdong Province (2024A1515012790).

COMPETING INTERESTS

The authors declare no competing interests.

ETHICS

The study was performed in accordance with the Declaration of Helsinki. All animal experimentation conducted in this investigation received approval from the Animal Ethics Review Committee of Shenzhen People's Hospital, and all procedural interventions strictly adhered to its stipulated guidelines. Collection of human samples was approved by the research ethics committee of Shenzhen People's Hospital. Each participant has signed an informed consent form.

ADDITIONAL INFORMATION

Supplementary information The online version contains supplementary material available at https://doi.org/10.1038/s41418-024-01371-w.

Correspondence and requests for materials should be addressed to Houqing Long or Songlin Peng.